$\chi^{(3)}$ Microscopic Techniques

Quan Wang

Optical Science and Engineering
University of New Mexico
Albuquerque, NM 87131

Microscopic techniques that utilize the third order non-linearality ($\chi^{(3)}$) of the sample have been the focus of active research in recent years. In this report, we first outline the principles of two widely used techniques: two photon excited fluorescent microscopy (TPEF) and coherent anti-Stokes Raman scattering microscopy (CARS) and then describe the working principles of a brand new kind of imaging technique: two-photon resonant enhanced stimulated parametric fluorescent (SPF) microscopy.

1. Introduction

Many biological samples are transparent, making them invisible in a conventional microscope. Varies methods have been proposed in the past century to circumvent such a hurdle. These include phase-contrast microscopy, dark-field microscopy, differential interference contrast microscopy, fluorescent imaging and so on. In 1990, W. Denk et, al [6] invented the two-photon excited fluorescent microscopy (TPEF) which greatly advanced imaging science. It was also the first microscopic technique that utilizes the third-order nonlinear susceptibility ($\chi^{(3)}$) of the sample. However, the main drawbacks of TPEF includes chemical staining and photo bleaching. Starting from the late 1990s, people began to investigate imaging methods based upon intrinsic nonlinear signals from the samples themselves. These include second harmonic generation (SHG) microscopy, third harmonic generation (THG) [12] microscopy and coherent anti-Stokes Raman scattering (CARS) microscopy [4, 5, 14]. The novel four-wave mixing microscopic being developed in our group which utilizes two-photon enhanced $\chi^{(3)}$ and stimulated parametric emission belongs to the same category. In what follows, we overview TPEF and CARS microscopy before describing in detail about the new stimulated parametric fluorescent microscopy.

2. Two-photon Excited Fluorescent Microscopy

The only difference between linear fluorescent imaging and TPEF is how the fluorophore is excited to a higher electronic state. In linear fluorescent microscopy, one photon of the "correct" energy is absorbed while in TPEF, a fluorophore molecule has a certain probability of absorbing two photons of lower energy simultaneously and reaches an excited electronic state. In the degenerated case (two photons of equal energy) the two-photon absorption coefficient β is directly related to the imaginary part of $\chi^{(3)}(\omega;\omega,\omega,-\omega)$ by the following relation [11],

$$\beta = \frac{\omega}{\epsilon_0 n_0^2 c^2} Im\{\chi^{(3)}(\omega;\omega,\omega,-\omega)\} \tag{1}$$

The two photon absorption (TPA) cross section is given in terms of β as,

$$\sigma_{2p} = \frac{\hbar\omega\beta}{N} \tag{2}$$

where N is the concentration of the fluorophore molecule. Note that too high a concentration might lead to fluorescence quenching. The law of absorption in the two-photon case (assuming no linear absorption) is

$$\frac{dI}{dz} = -\beta I^2 \tag{3}$$

After absorption, the molecule relaxes and then emits a photon as in linear fluorescent imaging. The emitted photon has a good chance of being captured by the collecting optics which help provide position information of the fluorophore.

One superb advantage of TPEF is its ability to do 3D sectioning. This can be best understood by studying the excitation dependency of the excitation process. TPA rate is proportional to excitation intensity squared (I^2). In a tight focus geometry, I^2 reaches significant value only at the focal volume, greatly reducing the sampling volume.

3. Coherent anti-Stokes Raman scattering Microscopy

Contrast in TPEF microscopy is provided by the added fluorophore. In wave-mixing microscopy (SHG, THG, CARS, SPF), signal originates from the sample itself, so the staining problem can be avoided. However, nonlinear processes are generally very weak, in order to have considerable amount of signal, there are two requirements: the interacting electric field has to be sufficiently strong (use of ultrashort pulses) and to take advantage of resonant enhancement of the susceptibilities.

CARS microscopy utilizes the rotational resonances of the molecules. Fig. 1(A) illustrates the energy diagram of CARS microscopy. In the actual experiment, there are two time-overlapped, pulsed laser sources (usually pico-second sources) providing $\omega_p = \omega_p'$ (pump) and ω_s (Stokes). For spectroscopy, the stokes beam ω_s is tunable, when the resonant enhancement condition is satisfied $\omega_p - \omega_s \approx \Omega$, where Ω is the angular frequency difference of two real vibrational states of the system, the probability of producing an anti-Stokes photon ω_{as} is hugely enhanced, resulting in a increased signal. In microscopy, the difference of pump and Stokes frequency is in agreement with the Raman band of the molecule of interest. (Fig. 2) Also shown in Fig. 1 is the phase matching condition of CARS, it's worth noting that because the focusing region is usually shorter than the coherent length, phase matching can be easily satisfied.

CARS microscopy is not background free, because $\chi^{(3)}(\omega_{as}; \omega_p, \omega_p, -\omega_s)$ is not zero (although small) when resonant condition is not met. In general, the susceptibility giving rise to $\vec{P}^{(3)}$ can be written as, [4]

$$\begin{aligned}\chi^{(3)}_{1111}(\omega_{as}; \omega_p, \omega_p, -\omega_s) = \eta_{NR} &+ \frac{A_t}{\omega_t - 2\omega_p - i\Gamma_t} \\ &+ \frac{A_t}{\omega_t - (\omega_p + \omega_s) - i\Gamma_t} \\ &+ \frac{A_t}{\omega_t - 2\omega_s - i\Gamma_t} \\ &+ \sum_R \left[\frac{A_R}{\Omega_R - (\omega_p - \omega_s) - i\Gamma_R}\right]\end{aligned} \tag{4}$$

where η_{NR} denotes the "residue" susceptibility which causes the background, A_t being the electronic resonant strength, A_R is the vibrational resonant strength and Γ describes damping associated with each resonance. In CARS microscopy, the samples are molecules whose

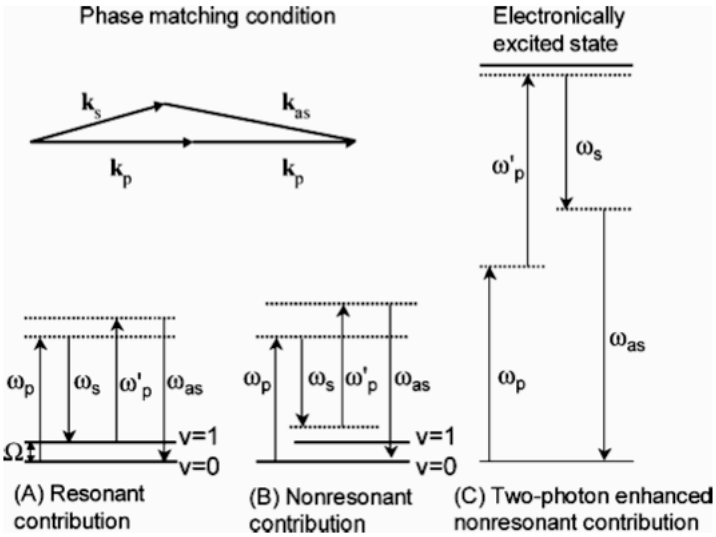

Fig. 1. Energy diagram of CARS [5]. (A) Resonant CARS, corresponding to $\omega_p - \omega_s \approx \Omega$. (B) Non-resonant contribution when $\omega_p - \omega_s$ deviates from Ω. (C) Electronic contribution, will be two-photon enhanced when $\omega_p + \omega'_p \approx \omega_t$.

electronic resonance are in the UV, so by setting the pump and Stokes beam to be in the near-IR ($800nm \sim 1000nm$), the electronic resonance terms in Eqn. 4 (the second, third and fourth terms) are kept reasonably small [14]. The contrast is provided only by the "signature" vibrational levels of the system (last term in Eqn. 4).

Due to its four-wave mixing nature, CARS signal depends quadratically on the pump beam intensity and linearly on the Stokes beam intensity ($I_{as} \propto I_p^2 I_s$), this means that the 3D sectioning capability is also present. Fig. 2 is an example of CARS microscopy.

4. Two-photon Enhanced Stimulated Parametric Fluorescent Microscopy

4.A. Theory

In CARS microscopy, the first four terms in Eqn. 4 are negligible compared to the rotational resonant term because the electronic transitions of molecules used in CARS are in the UV. However, if the sample is fluorescent dye which has reasonable two-photon absorption cross section in the IR, one or more of the electronic resonance terms in Eqn. 4 might come into resonance. For input frequencies ω_1 and ω_2, there are three ways that the two-photon resonant condition can be satisfied. These are,

$$2\omega_1 \approx \omega_t \quad \text{or} \quad 2\omega_2 \approx \omega_t \quad \text{or} \quad \omega_1 + \omega_2 \approx \omega_t \tag{5}$$

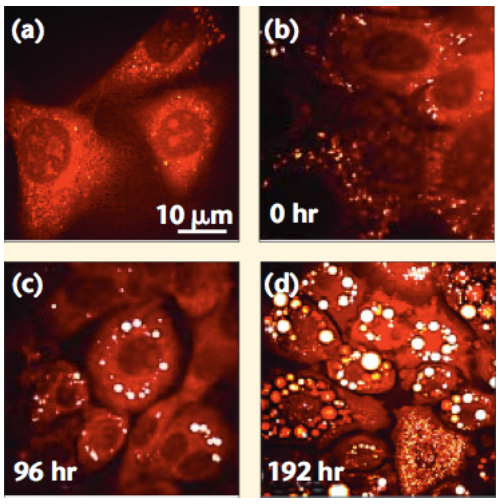

Fig. 2. Growth of lipid droplets in live cells monitored by CARS microscopy. Lipid contrast at 2845 cm^{-1} was used to visualize lipids without staining. [Adapted from [9]]

which correspond to three ways which four-wave mixing process might happen. Fig 3 shows the first two of them. (The third case doesn't generate new frequency component so are not of interest to us.) These processes are parametric processes.

It must be pointed out that in Fig 3(a), if $\omega_1 - \omega_2$ is in agreement with one of the Raman bands (last term in Eqn. 4), two-photon resonance and vibrational resonance happen at the same time and there is no way to tell which process dominates because they produce the same output frequency. However, the process described by Fig 3(b) has no CARS counterpart. The nonlinear susceptibility describing such a process is simply

$$\chi^{(3)}(\omega_{IR}; \omega_2, \omega_2, -\omega_1) = \chi^{NR} + \frac{A_t}{\omega_t - 2\omega_2 + i\Gamma_t} \tag{6}$$

where χ^{NR} summarizes all the non-resonant contribution. The subscript "IR" is used because in the experiment we set ω_1 and ω_2 to be $2\pi c/(800\ nm)$ and $2\pi c/(1100\ nm)$ respectively. The resulting photon $(2\omega_2 - \omega_1)$ is therefore in the infrared. We call this signal "IR-SPF".

4.B. Experiment

A mode-locked Ti:Sapphire laser ($80fs$, $100MHz$ repetition rate, $\lambda_1 \sim 850\ nm$) and a synchronously pumped OPO ($\lambda_2 \sim 1100\ nm$) are used as excitation sources. They are overlapped in time before being directed to a scanning microscope. The collecting objective has a numerical aperture of 0.4 and the collected signal is split into two detector channels, one for the IR-SPF signal, the other for the TPEF signal. The detector used for the IR-SPF

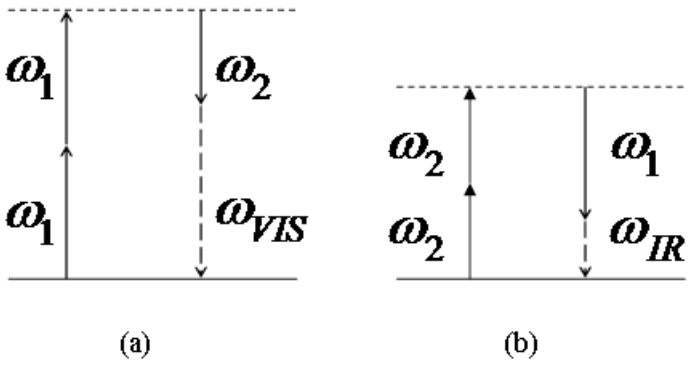

Fig. 3. Energy diagram of two-photon enhanced SPF. (a) the visible output (b) the IR output

signal is a InGaAS femto-watt IR detector (New Focus 2153). An avalanche photodiode (Hamamatsu C5460-01) is used to detect TPEF signal which is in the visible. Appropriate filters are placed in front of the detectors to eliminate excitation and SHG signals.

Fig. 5 shows the same field of view imaged by IR-SPF (left) and TPEF (right), the sample contains two kinds of polymer beads, one with R6G dye inside, the other one without. The TPEF image is taken by the OPO Beam (ω_2) only. (R6G has considerable two photon cross section at 1100 nm. [13]) It can be seen that only those with dye show up in both of the channels while those without the beads show up in the IR-SPF only, this is due to the non-resonant contribution (first term in Eqn. 6) from the polymer itself.

4.C. Polarization Sensitive Detection

It can be demonstrated that the non-resonant signal can be filtered out by polarization sensitive detection techniques. Similar techniques have been successfully used in CARS microscopy, [2, 10]. The trick is to allow two excitation beams to have different linear polarization (separated by ϕ, Fig. 6), because the non-resonant susceptibility is mostly real [1], the non-resonant (NR) signal is linearly polarized. The two-photon resonant enhanced signal, on the other hand, is elliptically polarized with a main axes different from the direction of the non-resonant signal), due to the imaginary component of the susceptibility near resonance. Therefore, a analyzer placed perpendicular to the NR polarization will eliminate the NR signal.

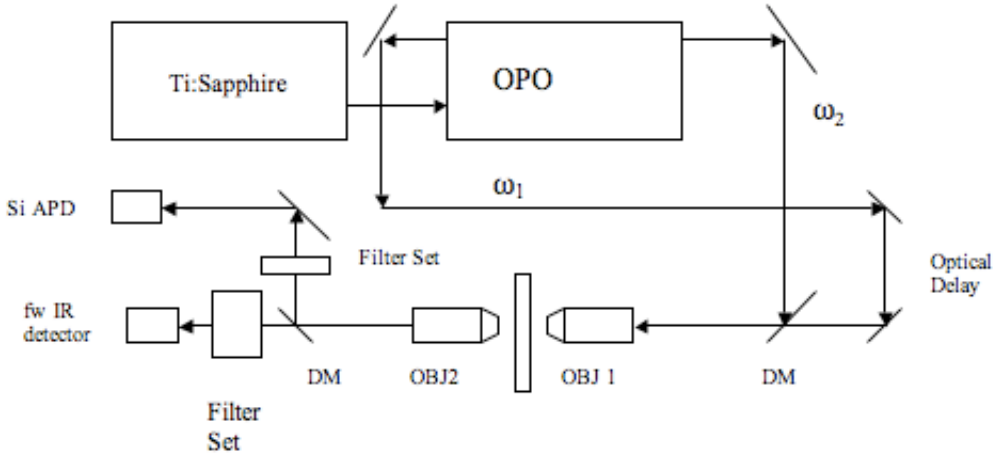

Fig. 4. Experimental setup [8]: DM, dichroic mirror

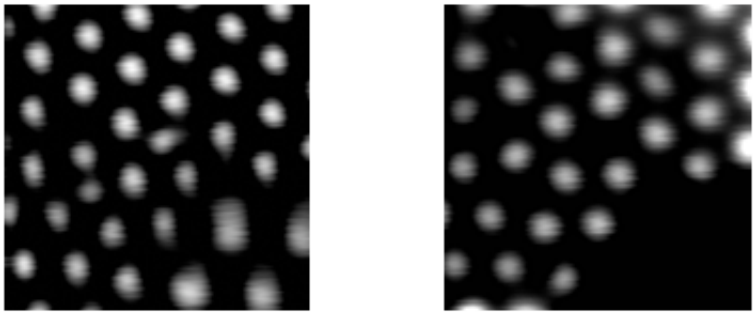

Fig. 5. Same field of view imaged by IR-SPF (left) and TPEF (right), the sample contains two kinds of polymer beads, one with R6G dye, the other one without. Those with dye show up in both TPEF and IR-SPF. Those without dye show up in the IR-SPF channel only. [personal communication [8]]

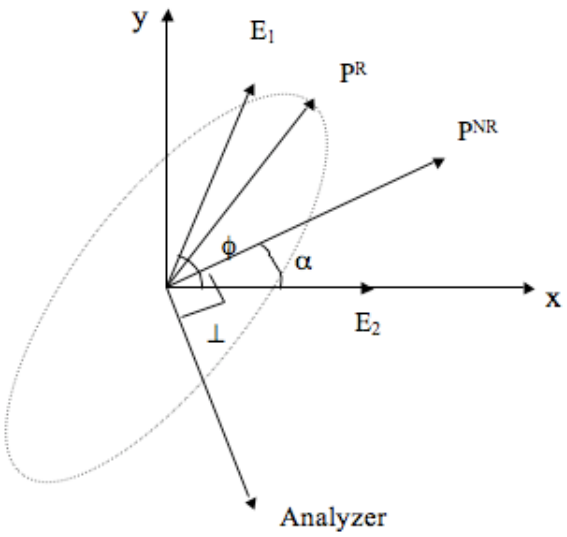

Fig. 6. Polarization sensitive detection. The non-resonant contribution to the IR-signal is linear polarized, an analyzer placed perpendicular to its polarization direction removes it.

5. Conclusions

In this report we have outlined two widely used microscopic techniques: TPEF depends on the imaginary part of $\chi^{(3)}(\omega;\omega,\omega,-\omega)$ to excite fluorophore to the excited state by two-photon absorption; CARS is a four-wave mixing process that is resonant-enhanced by the intrinsic rotational levels of the sample. It is also an ultrafast process that happens within a time scale of femto-second. The new imaging method (two-photon enhanced SPF) that we are currently investigating, can be thought of as a hybrid of the two, it is an ultrafast, four-wave mixing process that takes advantage of the two-photon resonant enhancement. With polarization sensitive detection, samples that works well under TPEF will show up in the IR-SPF channel as well. The biggest advantage of SPF over TPEF is that because of it is wave-mixing process, almost no real absorption occurs, thus photo bleaching might be prevented. Initial experiments of SPF on photo-bleaching show that the decay time of the signal is longer than the same sample under TPEF [8]. The details are still being investigated.

References

1. Boyd, R. W. *Nonlinear Optics 2nd edition.* Academic Press, 2003.
2. Cheng, J.-X., Book, L. D., and Xie, X. S. Polarization coherent anti-stokes raman scattering microscopy. *Opt. Lett. 26*, 17 (2001), 1341–1343.
3. Cheng, J.-X., Volkmer, A., Book, L. D., and Xie, X. S. An epi-detected coherent anti-stokes raman scattering (e-cars) microscope with high spectral resolution and high sensitivity. *J. Phys. Chem. B 105*, 7 (2001), 1277–1280.
4. Cheng, J.-X., Volkmer, A., and Xie, X. S. Theoretical and experimental characterization of coherent anti-stokes raman scattering microscopy. *J. Opt. Soc. Am. B 19*, 6 (2002), 1363–1375.
5. Cheng, J.-X., and Xie, X. S. Coherent anti-stokes raman scattering microscopy: Instrumentation, theory, and applications. *J. Phys. Chem. B 108* (2004), 827–840.
6. Denk, W., Strickler, J. H., and Webb, W. W. Two-photon laser scanning fluorescence microscopy. *Science 248* (1990), 73–76.
7. Isobe, K., Kataoka, S., Murase, R., Watanabe, W., Higashi, T., Kawakami, S., Matsunaga, S., Fukui, K., and Itoh, K. Stimulated parametric emission microscopy. *Opt. Exp. V14*, N2 (2006), 786–793.
8. Liu, X. Two photon enhanced stimulated parametric fluorescence microscopy. Unpublished.
9. Nan, X., Cheng, J.-X., and Xie, X. S. Vibrational imaging of lipid droplets in live fibroblast cells with coherent anti-stokes raman scattering microscopy. *J. Lipid Res. 44* (2003), 2202–2208.
10. Oudar, J.-L., Smith, R. W., and Shen, Y. R. Polarization-sensitive coherent anti-stokes raman spectroscopy. *Appl. Phys. Lett. 34*, 11 (1979), 759.
11. Sheik-Bahae, M., and Hasselbeck, M. P. *Third Order Optical Nonlinearities.* OSA, 2001.
12. Yelin, D., Oron, D., Korkotian, E., Segal, M., and Silberberg, Y. Third-harmonic microscopy with a titanium-sapphire laser. *Appl. Phys. B* (2002).
13. Zipfel, W. R., Williams, R. M., and Webb, W. W. Nonlinear magic: multiphoton microscopy in the biosciences. *Nature Biotechnology 21*, 11 (2003), 1369–1377.
14. Zumbusch, A., Holtom, G. R., and Xie, X. S. Three-dimensional vibrational imaging by coherent anti-stokes raman scattering. *Phys. Rev. Lett. 82*, 20 (1999), 4142–4145.